論文 / 著書情報
Article / Book Information

Title	Mapping subduction interface coupling using magnetotellurics; Hikurangi Margin, New Zealand
Authors	W. Heise, T. G. Caldwell, S. Bannister, E.A. Bertrand, Y. Ogawa, S.L. Bennie, H. Ichihara
Citation	Geophysical Research Letters, 44, 18, 9261–9266
Pub. date	2017, 9
DOI	http://dx.doi.org/10.1002/2017GL074641
Copyright	(c) 2017 American Geophysical Union (AGU)

AGU PUBLICATIONS

Geophysical Research Letters

RESEARCH LETTER
10.1002/2017GL074641

Key Points:
- Heterogeneous resistivity structure imaged on the plate interface on the Hikurangi subduction margin
- Resistivity structure correlates with plate coupling inferred by geodetic data
- The frictional coupling of the northern Hikurangi margin may be controlled by the interface fluid and sediment content

Supporting Information:
- Supporting Information S1

Correspondence to:
W. Heise,
w.heise@gns.cri.nz

Citation:
Heise, W., T. G. Caldwell, S. Bannister, E. A. Bertrand, Y. Ogawa, S. L. Bennie, and H. Ichihara (2017), Mapping subduction interface coupling using magnetotellurics: Hikurangi margin, New Zealand, *Geophys. Res. Lett.*, *44*, 9261–9266, doi:10.1002/2017GL074641.

Received 19 JUN 2017
Accepted 21 AUG 2017
Accepted article online 25 AUG 2017
Published online 19 SEP 2017

Mapping subduction interface coupling using magnetotellurics: Hikurangi margin, New Zealand

W. Heise[1], T. G. Caldwell[1], S. Bannister[1], E. A. Bertrand[1], Y. Ogawa[2], S. L. Bennie[1], and H. Ichihara[3,4]

[1]GNS Science, Lower Hutt, New Zealand, [2]Volcanic Fluid Research Center, Tokyo Institute of Technology, Tokyo, Japan, [3]Institute for Research on Earth Evolution, Japan Agency for Marine-Earth Science and Technology, Yokosuka, Japan, [4]Now at Earthquake and Volcano Research Center, Graduate School of Environmental Studies, Nagoya University, Nagoya, Japan

Abstract The observation of slow-slip, seismic tremor, and low-frequency earthquakes at subduction margins has provided new insight into the mechanisms by which stress accumulates between large subduction (megathrust) earthquakes. However, the relationship between the physical properties of the subduction interface and the nature of the controls on interplate seismic coupling is not fully understood. Using magnetotelluric data, we show in situ that an electrically resistive patch on the Hikurangi subduction interface corresponds with an area of increased coupling inferred from geodetic data. This resistive patch must reflect a decrease in the fluid or sediment content of the interface shear zone. Together, the magnetotelluric and geodetic data suggest that the frictional coupling of this part on the Hikurangi margin may be controlled by the interface fluid and sediment content: the resistive patch marking a fluid- and sediment-starved area with an increased density of small, seismogenic-asperities, and therefore a greater likelihood of subduction earthquake nucleation.

1. Introduction

Along the Hikurangi subduction margin on the east coast of New Zealand's North Island (Figure 1), a large oceanic plateau on the Pacific plate with anomalously thick crust is being subducted beneath continental crust of the Australian plate. This causes the plate interface to lie at shallow (15–30 km) depths beneath the North Island's east coast [*Reyners et al*., 1999; *Williams et al*., 2013], allowing processes occurring at the subduction interface to be investigated using land-based geophysical techniques. Geodetic data from the northern part of the Hikurangi margin show that interplate coupling is weak in this part of the margin and that large slow-slip events (with slip areas equivalent to the rupture area of an *M* 6.3–7.2 earthquake) occur just offshore approximately every 2 years [*Wallace and Beavan*, 2010; *Wallace et al*., 2012, 2016]. Farther to the south, beneath the southern part of the North Island, the subduction interface is locked (Figure 1 inset) [*Wallace and Beavan*, 2010].

Magnetotelluric (MT) surveys from the northern part of the Hikurangi margin show that an electrically conductive zone is present above the subducting plate [*Heise et al*., 2012, 2013]; the high conductance interpreted to be the result of fluids and clay-rich sediment in the interface shear zone. However, MT results from a single line of measurements in the locked part of the margin 350 km to the south did not image a conductive zone above the plate, suggesting a possible correlation between plate coupling and the electrical resistivity of the interface shear zone [*Heise et al*., 2013].

Plate coupling depends on factors such as the temperature, composition, pore pressure, and fluid content of the interface shear zone [e.g., *Saffer and Wallace*, 2015]. Any heterogeneity of the seismic coupling must reflect variation of some or all of these factors. Also, if the plate interface is rough, weaker fluid- and clay-rich sediment patches may be interspersed among more strongly coupled regions starved of fluid and sediment [*Wang and Bilek*, 2011]. In particular, these authors argue that large scale (~10 km) frictional heterogeneities will be associated with subducted seamounts present at tectonically erosive subduction margins like the northern part of the Hikurangi subduction zone [*Bell et al*., 2014; *Wallace et al*., 2016]. Geological evidence for variations in interface sediment and fluid content playing an important role in subduction interface frictional coupling can also be found in an exhumed example of a subduction interface shear zone in the western part of the European Alps [*Bachmann et al*., 2009]. High

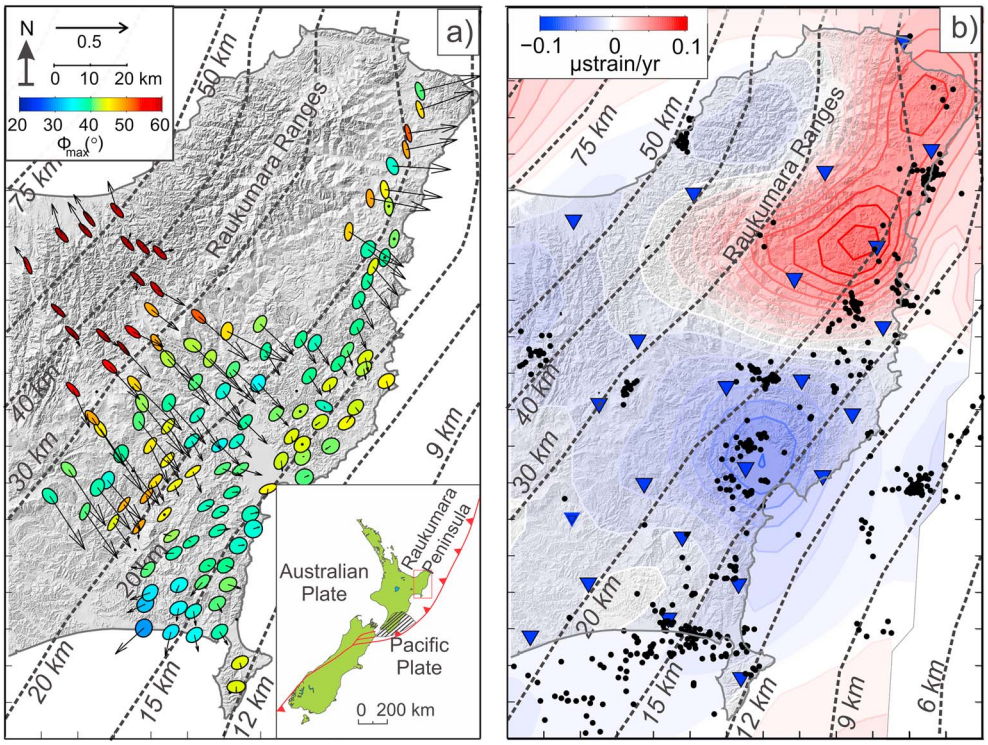

Figure 1. MT data, near-interface seismicity, and areal strain rate. Inset shows tectonic context with major plate bounding faults shown in red. The hatched region marks the area where the subduction interface beneath the southern tip of the North Island is locked. Dashed lines show the depth to the plate interface [*Williams et al*., 2013]. (a) MT phase tensor ellipses and induction vectors (real part) at 85 s period. The tensor ellipses have been normalized by their maximum principal value (Φ_{max}), ellipse color indicating the magnitude of Φ_{max}. Induction arrows are shown such that vectors point toward regions of high conductance. (b) Areal strain map derived from GPS measurements, warm colors indicating extension and cold colors contraction. The blue area in the center of the map is consistent with increased frictional coupling on the plate interface [*Dimitrova et al*., 2016]. Blue triangles show the locations of continuously recording GPS stations and the black dots show seismicity located within 1 km of the plate interface.

pore pressure fluids in subduction zones inferred from high V_p/V_s ratios have also been linked to conditionally stable areas and slow-slip events in Japan and elsewhere [e.g., *Kodaira et al*., 2004; *Saffer and Tobin*, 2011] consistent with theoretical expectations [*Scholz*, 1998].

To test the idea that the subduction interface coupling is correlated with the electrical resistivity of the interface shear zone, a proxy for fluid and sediment content, we invert MT data from an array of 132 MT measurements sites, which were located in the weakly coupled part of the Hikurangi margin (Figure 1). We then compare the MT results with earthquake and geodetic data from the same area.

2. MT Data

The MT method uses surface measurements of naturally occurring, low-frequency variations of the magnetic field at the Earth's surface and the electric field induced by the variations to create an image of the subsurface electrical resistivity [*Chave and Jones*, 2012]. The depth to which the induced electromagnetic (EM) fields penetrate depends on both the overlying resistivity distribution and the period of the variations, penetration depth increasing with increasing period.

Magnetic and electric field time series were recorded over 2 days with typical acquisition times at each measurement site of 40 to 50 h. Standard remote reference MT data processing techniques [*Chave and Jones*, 2012] (as implemented by Phoenix Geophysics) were used to convert each EM field component time series into the frequency domain.

In the frequency domain, the MT data are represented by a four-component (complex) impedance tensor **Z** and a two-component (complex) induction vector **K**. These quantities express the (normalized) magnitude

and phase relations between the surface EM field components and are defined by the equations $\mathbf{E}(\omega) = \mathbf{Z}(\omega)\mathbf{H}(\omega)$ and $H_z(\omega) = -\mathbf{K}(\omega)\mathbf{H}(\omega)$, where **E** and **H** are the horizontal electric and magnetic field vectors, H_z is the vertical component of the magnetic field, $\omega = 2\pi/T$ is the angular frequency, and T is the period. Hourly stacks of the EM field component crosspowers were used to calculate impedance tensor (**Z**) and induction vector (**K**) data used as inputs for the MT data inversion.

While the amplitude information contained in **Z** is subject to the distorting effects produced by localized near-surface resistivity heterogeneities, the phase information is unaffected. The phase relationships contained in **Z** can be expressed as a tensor [*Caldwell et al*., 2004] defined by the equation $\mathbf{\Phi} = \mathbf{X}^{-1}\mathbf{Y}$, where **X** and **Y** are the real and imaginary parts of **Z**, respectively, and **Φ** is independent of (galvanic) distortion. Graphically the phase tensor **Φ** can be represented as an ellipse with principal (ellipse) axes Φ_{max} and Φ_{min}. Maps of the phase tensor ellipses provide a way of visualizing the lateral resistivity changes in a depth range that is (nonlinearly) dependent on the period and overlying resistivity. Differences in the lengths of the tensor ellipse (principal) axes indicate the magnitude and orientation of lateral resistivity gradients present in the depth range concerned. Similarly, the induction vectors point toward areas of greater conductance along the direction of the gradient in the conductance.

A map of the phase tensor ellipses and induction vectors at 85 s period is shown in Figure 1a where the color fill of the ellipse is used to indicate the magnitude of the maximum principal phase Φ_{max}. For this part of the Hikurangi margin, the MT data at 85 s period (Figure 1a) are sensitive to resistivity gradients where the depth is between 15 and 25 km. In Figure 1a, Φ_{max} phase changes by about 10° in the central part of the survey, parallel to the subduction-interface depth contours. This change indicates significant along-strike resistivity gradients at depths comparable with the interface.

3. Earthquake and Geodetic Data

Epicenters of earthquakes with magnitudes greater than 1 and that lie within 1 km of the subduction interface [*Williams et al*., 2013] are plotted in Figure 1b. Hypocenters of these earthquakes that were recorded by New Zealand's national seismometer network (www.geonet.org.nz) between 2001 and 2012 were located using a 3-D velocity model specifically developed for the northern Hikurangi subduction margin [*Eberhart-Phillips et al*., 2010]. The largest magnitude event in this subset of earthquakes was 3.9. The small clusters of seismicity observed suggest that localized asperities are present on the interface that breaks in small earthquakes. Episodic bursts of seismic tremor, thought to be generated by episodes of localized slip in the interface shear zone too small to be resolved geodetically [*Wech and Creager*, 2011], have also been reported along this part of the Hikurangi margin [*Todd and Schwartz*, 2016] (supporting information Figure S1).

Also shown in Figure 1b is a map of the areal-strain rate derived from an inversion of the GPS velocity field derived from GPS data recorded between 1995 and 2013 [*Haines et al*., 2015; *Beavan et al*., 2016; *Dimitrova et al*., 2016]. The area of contractive areal-strain rate centered on the 20 km interface depth contour [*Williams et al*., 2013] is consistent with the presence of a more strongly coupled patch on the plate interface [*Dimitrova et al*., 2016].

4. MT Inverse Modeling

Where a phase tensor analysis of the MT data shows that the impedance response at short periods is one-dimensional, the phase mixing effects of galvanic distortion can be removed from the impedance tensor [*Bibby et al*., 2005] prior to data inversion. The phase mixing effects of distortion could be identified at 124 of the 132 MT measurement locations. These effects were removed from the impedance tensors at these sites, and the (corrected) impedance tensor and induction vector data were then inverted using a parallelized version of the 3-D MT inversion code of *Siripunvaraporn and Egbert* [2009]. More details of the inversion methodology are given in the supporting information.

Given an initial model of the resistivity, the inversion algorithm used in this code searches for the smoothest resistivity distribution that best fits the data within a given error tolerance. Including a priori information into the initial resistivity model helps convergence. Our initial model (Figure S2) included a simplified model of the

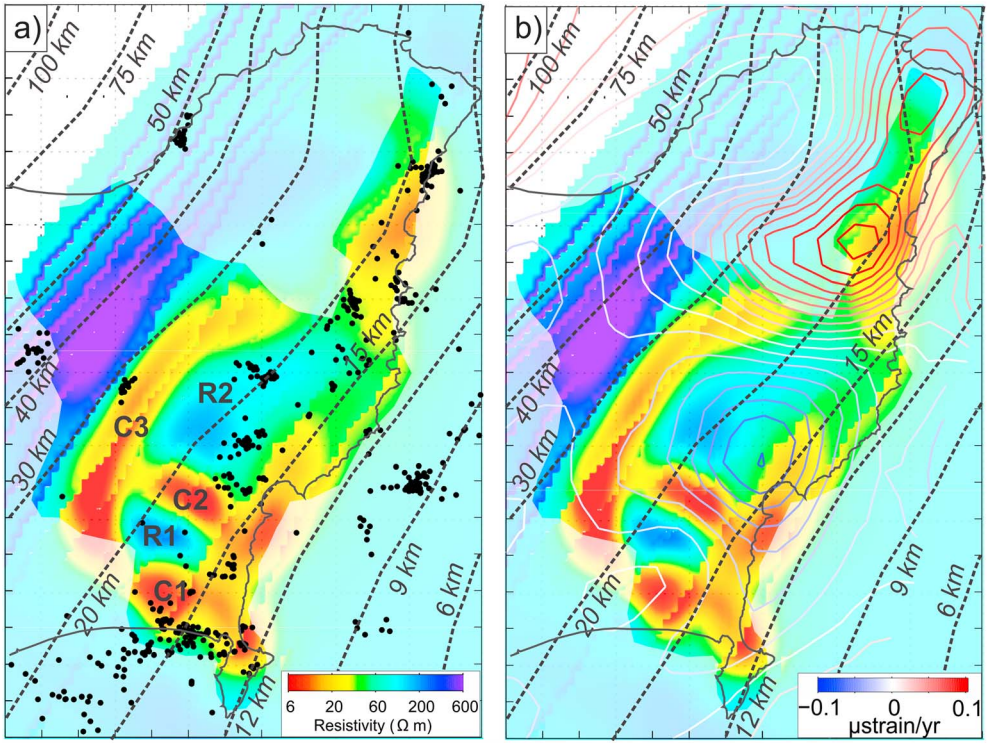

Figure 2. Resistivity at the plate interface with near interface seismicity and areal strain rate superimposed. Pale colors indicate the area where the resistivity model is not well constrained by MT data coverage. Dashed lines show the depth contours of the plate interface. (a) Seismicity (black dots) located within 1 km of the plate interface. (b) Contours of areal strain rate [*Dimitrova et al*., 2016]. Main features are conductors C1, C2, and C3 interpreted as fluid- and/or clay-rich sediments; resistors R1 and R2 represent fluid and sediment poorer areas on the plate interface.

surrounding ocean and accreted sediments with a dipping resistive (500 Ωm) layer representing the down-going slab with geometry based on active-source seismic data [*Barker et al*., 2009; *Williams et al*., 2013].

Results from the 3-D inversion modeling are shown in Figures 2 and 3. These figures depict the resistivity at the depth estimated for the plate interface by *Williams et al*. [2013], with the near-interface seismicity and contours of areal strain rate superimposed in Figure 2. Between 15 and 30 km depth the resistivity near the plate interface varies by about an order of magnitude along the strike of the subduction margin. Hypothesis testing (supporting information) confirms that the conductive and resistive heterogeneities at the depth of the interface shown in Figures 2 and 3 are required by the MT data. However, inversions using different initial models show that the MT data lack the resolution to distinguish whether or not the conductive zone extends into the oceanic crust of the down going plate (supporting information).

The SW-NE trending band of higher conductance (C3 in Figure 2) between 25 and 30 km depth is interpreted to mark the base of a body of underplated sediments undergoing low-grade prograde metamorphism [*Heise et al*., 2012]. Seismic tomography shows low *P* wave speed, high *P* wave to *S* wave velocity ratios and higher levels of *P* wave attenuation in the same region [*Reyners et al*., 1999; *Eberhart-Phillips and Bannister*, 2015] (Figure S4). Rapid uplift of the Raukumara Ranges (Figure 1) is also believed to be a consequence of sediment underplating [*Walcott*, 1987]. The downdip limit of the conductive band (C3) corresponds well with Moho depth [*Eberhart-Phillips et al*., 2005; *Bassett et al*., 2010], consistent with the idea that underplated sediments in this part of the Hikurangi margin are not subducted below the Moho [*Sutherland et al*., 2009].

5. Discussion and Conclusions

Updip of the conductive band (C3), the interface resistivity is heterogeneous, with two resistive patches (R1 and R2 in Figure 2) surrounded by narrow areas of higher conductance (C1 and C2 in Figure 2). These areas appear to be downdip continuations of the broad area of high to intermediate conductance at depths

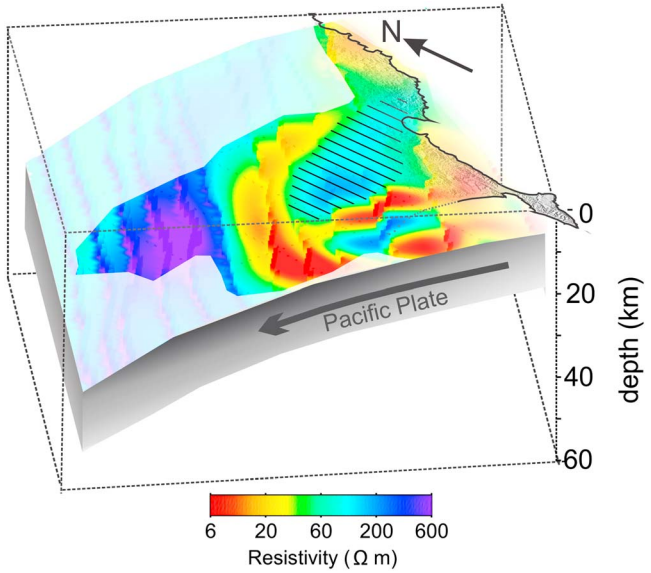

Figure 3. Three-dimensional view of resistivity on the plate interface. The hatched area shows the patch of the interface with reduced fluid or sediment content interpreted as a region with increased frictional coupling.

shallower than 15 km, which were interpreted by *Heise et al.* [2012, 2013] to be fluid- and clay-rich sediments within the interface shear zone. Conductors C1 and C2 appear to show regions where fluid- and/or clay-rich sediment is entrained, possibly related to subduction interface relief, the conductive regions representing zones of greater sediment thickness or fluid content related to overpressured fluids and/or metamorphic fluid production [*Heise et al.*, 2013].

The most plausible explanation for the resistive patches (R1 and R2 in Figure 2) is that they mark areas of the interface shear zone with reduced fluid or sediment content. If so, we might expect frictional coupling to be greater in the resistive areas. An area of increased frictional coupling comparable in size (~1500 km^2) with R2 should also produce a measurable geodetic signal at the surface. The correlation between the area of contractive strain rate seen in the geodetic data and the resistive patch (Figure 2b) is remarkable and provides evidence that the resistive patch is indeed an area of increased inter-plate coupling. To our knowledge, this is the first time that such a close correlation between MT and geodetic data has been reported; however, previous 2-D MT studies at the Cascadia margin showed correlation between plate locking and resistivity [*Wannamaker et al.*, 2014].

Together the MT and geodetic data inversions suggest that the subduction interface coupling in the northern Hikurangi margin is controlled by the fluid and sediment content of the interface shear zone. These results, along with the clustered nature of the interface seismicity and the broad distribution of seismic tremor, support the concept of the subduction interface as a mosaic of locked, creeping and slow-slipping patches at a wide variety of length scales. This concept has also been used to explain the association between slow-slip events and seismic tremor observed at subduction margins around the Pacific Rim [*Dragert et al.*, 2001; *Wech and Creager*, 2011; *Shelly et al.*, 2007; *Obara and Kato*, 2016].

The resistive patch on the interface appears to mark an area with an increased density of asperities and stored strain. These factors will enhance the likelihood that a rupture of a single asperity in this patch will cascade into a large earthquake, ~*M* 7.5 if the entire resistive patch ruptured in a single event [*Murotani et al.*, 2008]. Our results suggest that fluid- and sediment-poor regions of the interface large enough to nucleate a subduction earthquake with magnitude 7.5 or greater can be resolved by MT. Images of the electrical resistivity of the subduction interface provide a method for helping determine the nature and distribution of frictional coupling on the subduction interface.

Acknowledgments

Our thanks go to W. Siripunvarporn for making his 3-D inverse MT modeling code available and to Laura Wallace and John Haines for sharing their analysis of the geodetic data. Comments by Damian Saffer and an anonymous reviewer helped to correct a number of our misunderstandings and improved the manuscript. Nick Cozens, Graham Hill, and Erin Wallin participated in the initial stages of MT data collection. This work was supported by GNS Science's direct Crown funded research and the Royal Society of New Zealand Marsden fund. Strain rate data shown in Figure 1b are from *Dimitrova et al.* [2016] *New Zeal. J. Geol. Geop.*, *59:1*, *43-57*, *doi:10.1080/00288306.2015.1127823*. Three-dimensional resistivity model data and earthquake locations shown in Figures 2 and 3 are available from Mendeley Data doi:10.17632/5cbbbxvxyh.1. Original MT data may be obtained by the authors (w.heise@gns.cri.nz) on a case-by-case basis.

References

Bachmann, R., O. Oncken, J. Glodny, W. Seifert, V. Georgieva, and M. Sudo (2009), Exposed plate interface in the European Alps reveals fabric styles and gradients related to an ancient seismogenic coupling zone, *J. Geophys. Res.*, *114*, B05402, doi:10.1029/2008JB005927.

Barker, D. H. N., R. Sutherland, S. Henrys, and S. Bannister (2009), Geometry of the Hikurangi subduction thrust and upper plate, North Island, New Zealand, *Geochem. Geophys. Geosyst.*, *10*, Q02007, doi:10.1029/2008GC002153.

Bassett, D., R. Sutherland, S. Henrys, T. Stern, M. Scherwath, A. Benson, S. Toulmin, and M. Henderson (2010), Three-dimensional velocity structure of the northern Hikurangi margin, Raukumara, New Zealand: Implications for the growth of continental crust by subduction erosion and tectonic underplating, *Geochem. Geophys. Geosyst.*, *11*, Q10013, doi:10.1029/2010GC003137.

Beavan, J., L. M. Wallace, N. Palmer, P. Denys, S. Ellis, N. Fournier, S. Hreinsdottir, C. Pearson, and M. Denham (2016), New Zealand GPS velocity field: 1995–2013, *New Zeal. J. Geol. Geophys.*, *59*(1), 5–14, doi:10.1080/00288306.2015.1112817.

Bell, R., C. Holden, W. Power, X. Wang, and G. Downes (2014), Hikurangi margin tsunami earthquake generated by slow seismic rupture over a subducted seamount, *Earth Planet. Sci. Lett.*, *397*, 1–9, doi:10.1016/j.epsl.2014.04.005.

Bibby, H. M., T. G. Caldwell, and C. Brown (2005), Determinable and non-determinable parameters of galvanic distortion in magnetotellurics, *Geophys. J. Int.*, *163*, 915–930.

Caldwell, T. G., H. M. Bibby, and C. Brown (2004), The magnetotelluric phase tensor, *Geophys. J. Int.*, *158*, 457–469.

Chave, A. D., and A. G. Jones (Eds.) (2012), *The Magnetotelluric Method: Theory and Practice*, Cambridge Univ. Press, Cambridge, U. K.

Dimitrova, L. L., L. M. Wallace, A. J. Haines, and C. A. Williams (2016), High-resolution view of active tectonic deformation along the Hikurangi subduction margin and the Taupo Volcanic Zone, New Zealand, *New Zeal. J. Geol. Geop.*, *59*(1), 43–57, doi:10.1080/00288306.2015.1127823.

Dragert, H., K. Wang, and T. S. James (2001), A silent slip event on the deeper Cascadia subduction interface, *Science*, *292*(5521), 1525–1528, doi:10.1126/science.1060152.

Eberhart-Phillips, D., and S. Bannister (2015), 3-D imaging of the northern Hikurangi subduction zone, New Zealand: Variations in subducted sediment, slab fluids and slow slip, *Geophys. J. Int.*, *201*(2), 838–855, doi:10.1093/gji/ggv057.

Eberhart-Phillips, D., M. E. Reyners, M. P. Chadwick, and J.-M. Chiu (2005), Crustal heterogeneity and subduction processes: 3-D V_P, V_P/V_S and Q in the southern North Island, New Zealand, *Geophys. J. Int.*, *162*(1), 270–288.

Eberhart-Phillips, D., M. Reyners, S. Bannister, M. Chadwick, and S. Ellis (2010), Establishing a versatile 3-D seismic velocity model for New Zealand, *Seismol. Res. Lett.*, *81*, 992–1000.

Haines, A. J., L. Dimitrova, L. Wallace, and C. Williams (2015), *Enhanced Surface Imaging of Crustal Deformation: Obtaining Tectonic Force Fields Using GPS Data*, Springer, Germany.

Heise, W., T. G. Caldwell, G. J. Hill, S. L. Bennie, and E. A. Bertrand (2012), Magnetotelluric imaging of fluid processes at the subduction interface of the Hikurangi margin, New Zealand, *Geophys. Res. Lett.*, *39*, L04308, doi:10.1029/2011GL050150.

Heise, W., T. G. Caldwell, E. A. Bertrand, G. J. Hill, S. L. Bennie, and Y. Ogawa (2013), Changes in electrical resistivity track changes in tectonic plate coupling, *Geophys. Res. Lett.*, *40*, 5029–5033, doi:10.1002/grl.50959.

Kodaira, S., T. Iidaka, A. Kato, J.-O. Park, T. Iwasaki, and Y. Kaneda (2004), High pore fluid pressure may cause silent slip in the Nankai Trough, *Science*, *304*, 1295–1299.

Murotani, S., H. Miyake, and K. Koketsu (2008), Scaling of characterized slip models for plate-boundary earthquakes, *Earth Planets Space*, *60*, 987–991.

Obara, K., and A. Kato (2016), Connecting slow earthquakes to huge earthquakes, *Science*, *353*(6296), 253–257, doi:10.1126/science.aaf1512.

Reyners, M. E., D. Eberhart-Phillips, and G. Stuart (1999), A three-dimensional image of shallow subduction: Crustal structure of the Raukumara Peninsula, New Zealand, *Geophys. J. Int.*, *13*, 873–890.

Saffer, D. M., and H. J. Tobin (2011), Hydrogeology and mechanics of subduction zone forearcs: Fluid flow and pore pressure, *Annu. Rev. Earth Planet. Sci.*, *39*, 157–186.

Saffer, D., and L. M. Wallace (2015), The frictional, hydrologic, metamorphic and thermal habitat of shallow slow earthquakes, *Nat. Geosci.*, *8*, 594–600, doi:10.1038/ngeo2490.

Scholz, C. H. (1998), Earthquakes and friction laws, *Nature*, *391*, 37–42, doi:10.1038/34097.

Shelly, D. R., G. C. Beroza, and S. Ide (2007), Non-volcanic tremor and low-frequency earthquake swarms, *Nature*, *446*(7133), 305–307.

Siripunvaraporn, W., and G. Egbert (2009), WSINV3DMT: Vertical magnetic field transfer function inversion and parallel implementation, *Phys. Earth Planet. Inter.*, *173*, 317–329.

Sutherland, R., et al. (2009), Reactivation of tectonics, crustal underplating, and uplift after 60 Myr of passive subsidence, Raukumara Basin, Hikurangi-Kermadec fore arc, New Zealand: Implications for global growth and recycling of continents, *Tectonics*, *28*, TC5017, doi:10.1029/2008TC002356.

Todd, E. K., and S. Y. Schwartz (2016), Tectonic tremor along the northern Hikurangi margin, New Zealand, between 2010 and 2015, *J. Geophys. Res. Solid Earth*, *121*, 8706–8719, doi:10.1002/2016JB013480.

Walcott, R. I. (1987), Geodetic strain and the deformational history of the North Island during the late Cainozoic, *Philos. Trans. R. Soc. Lond.*, *A321*, 163–181.

Wallace, L. M., and R. J. Beavan (2010), Diverse slow slip behavior at the Hikurangi subduction margin, New Zealand, *J. Geophys. Res.*, *115*, B12402, doi:10.1029/2010JB007717.

Wallace, L. M., R. J. Beavan, S. Bannister, and C. A. Williams (2012), Simultaneous long-term and short-term slow slip events at the Hikurangi subduction margin, New Zealand: Implications for processes that control slow slip event occurrence, duration, and migration, *J. Geophys. Res.*, *117*, B11402, doi:10.1029/2012JB009489.

Wallace, L. M., S. C. Webb, Y. Ito, K. Mochizuki, R. Hino, S. Henrys, S. Y. Schwartz, and A. F. Sheehan (2016), Slow slip near the trench at the Hikurangi subduction zone, New Zealand, *Science*, *352*, 701–704.

Wang, K., and S. L. Bilek (2011), Do subducting seamounts generate or stop large earthquakes?, *Geology*, *39*, 819–822, doi:10.1130/G31856.1.

Wannamaker, P. E., R. L. Evans, P. A. Bedrosian, M. J. Unsworth, V. Maris, and R. S. McGary (2014), Segmentation of plate coupling, fate of subduction fluids, and modes of arc magmatism in Cascadia, inferred from magnetotelluric resistivity, *Geochem. Geophys. Geosyst.*, *15*, 4230–4253, doi:10.1002/2014GC005509.

Wech, A. G., and K. C. Creager (2011), A continuum of stress, strength and slip in the Cascadia subduction zone, *Nat. Geosci.*, *4*, 624–628, doi:10.1038/ngeo1215.

Williams, C. A., D. Eberhart-Phillips, S. Bannister, D. H. Barker, S. Henrys, M. Reyners, and R. Sutherland (2013), Revised interface geometry for the Hikurangi Subduction Zone, New Zealand, *Seismol. Res. Lett.*, *84*, 1066–1073.